

SEISMIC FRAGILITY ASSESSMENT OF HIGH-RISE STACKS IN OIL REFINERIES

N. D. Karaferis^{1*}, A. K. Kazantzi², V. E. Melissianos³, K. Bakalis⁴ and D. Vamvatsikos⁵

¹*Ph.D. Candidate, School of Civil Engineering, National Technical University of Athens, Athens, Greece.*

²*Senior Risk Engineer, Resilience Guard GmbH, Steinhausen, Switzerland.*

³*Research Associate, School of Civil Engineering, National Technical University of Athens, Athens, Greece.*

⁴*Research Associate, School of Civil Engineering, National Technical University of Athens, Athens, Greece.*

⁵*Associate Professor, School of Civil Engineering, National Technical University of Athens, Athens, Greece.*

Keywords: Oil refinery; Seismic fragility; High-rise stacks; Process tower; Chimney; Flare

Abstract: The seismic fragility is assessed for typical high-rise stacks encountered in oil refineries, namely process towers, chimneys, and flares. Models of varying complexity were developed for the structures of interest, attempting to balance computational complexity and accuracy regarding the structural dynamic and strength properties. The models were utilized along with a set of hazard-consistent ground motions for evaluating the seismic demands through incremental dynamic analysis. Demand/capacity-related uncertainties were explicitly accounted for in the proposed framework. Damage states were defined for each of the examined structure considering characteristic serviceability and ultimate limit states. The proposed resource-efficient roadmap for the analytical seismic fragility assessment of typical high-rise stacks, as well as the findings of the presented research work are available to be exploited in seismic risk assessment studies of oil refineries.

1. INTRODUCTION

Oil refineries are in the core of the fossil fuel production chain, playing a vital socioeconomic role since they affect a spectrum of parameters related to the economy and the communities in their proximity. Hence, safeguarding the integrity of these critical infrastructures in the aftermath of natural hazard-related events is of paramount importance in compliance with the Sendai Framework for Disaster Risk Reduction 2015-2030 (United Nations, 2015). To accomplish this goal, there is an emerging need for the development of a state-of-the-art holistic framework not only for evaluating the structural integrity and vulnerability of the individual critical assets against several natural and man-made perils, but also for enabling an efficient, practical, and robust risk-aware assessment of the refinery plant as an integrated system. Despite the advancements in the seismic design and construction practices, the seismic hazard remains a critical concern for oil refinery structures, since catastrophic failures are still occurring. Such natural-technological (NaTech) accidents in refineries (e.g. Godoy 2007; Hatayama 2008; Girgin 2011; Bi *et al.* 2021; Krausmann and Cruz 2021) often

* Corresponding author *Email: nkaraferis@mail.ntua.gr*

involve various types of critical asset structural failures that could eventually lead to the disruption of the facility's operations or even to more devastating consequences, such as injuries and fatalities, environmental pollution, and severe economic losses extending well beyond the loss of revenue.

A variety of structural typologies are typically encountered in an oil refinery, including liquid storage tanks, pressure vessels, piping, pipe-racks, process towers, open-frame buildings supporting industrial equipment, chimneys, process towers, auxiliary buildings, and flares. These structures possess fundamentally dissimilar geometrical and dynamic characteristics, thus the needed level of detail in their analytical representation within a seismic performance assessment framework is likely to vary considerably. Among the structural typologies encountered, the basis to evaluate the seismic performance via rigorous or reduced-order numerical models exists for only a limited number of them. In particular, past analytical seismic fragility assessment studies have been focused on liquid storage tanks (e.g. Bakalis *et al.* 2017; Spritzer and Guzey 2017; Vathi *et al.* 2017; Phan *et al.* 2020; Bakalis and Karamanos 2021; Yu and Whittaker 2021), pipe-racks (e.g. Bursi *et al.* 2018; Di Sarno and Karagiannakis 2021; Farhan and Bousias 2020; Zhang *et al.* 2021), and pressure vessels (e.g. Patkas and Karamanos 2007; Karakostas *et al.* 2015). On the other hand, the seismic fragility of typical high-rise stacks, i.e. process towers, chimneys, and flare stacks, has not received the same level of attention from the research community. A handful of studies is available on the seismic fragility of reinforced concrete (RC) chimneys via numerical models (e.g. Huang *et al.* 2004; Gould and Huang 2006; Zhou *et al.* 2015, 2019; Guo *et al.* 2018, 2019; Qiu *et al.* 2020), while contributions on steel chimneys and process towers are very scarce (e.g. Lopez *et al.* 1996; Moharrami and Amini 2014). Research on flare stacks to date is mainly focused on the wind hazard (e.g. Sheng *et al.* 2016; Liu 2017). This comes as no surprise since earthquakes are not the primary cause of catastrophic failures when it comes to high-rise stacks compared to wind loading (Wang and Fan 2019). Nevertheless, refineries are classified as critical facilities and hence their undisrupted operation against a spectrum of perils, including earthquakes, should be ensured to comply with the strict national and international safety regulations.

Owing to the above, a set of typical high-rise stacks encountered in an oil refinery is examined, attempting to fill the pertinent gap in the literature. In particular, the structural typologies examined herein comprise (a) a 30m high process tower, (b) a 30m high steel chimney, (c) an 80m high steel chimney, (d) an 87m high reinforced concrete chimney, and (e) a 67m high flare structure. Schematic illustrations of these structures are presented in Fig. 1(a-d). Since non-seismic loads (such as wind, or internal pressures) govern design, these structures are not necessarily specific to any region and may be considered as staples of many refineries, at least for sites where hurricane-strength winds are not a major hazard. Where possible, reduced-order models were developed for the aforementioned structures to reliably capture the most characteristic failure modes with less computational effort. In other cases, more refined models were required to achieve a satisfactory level of accuracy. For each one of those assets, suitable Damage States (DS) were defined, representative of characteristic failure modes that are likely to be encountered at increasing levels of the seismic intensity measure (*IM*), along with the associated Limit States (LS) capacity thresholds that signal exceedance. The induced seismic demands were computed by means of Incremental Dynamic Analyses (IDA) (Vamvatsikos and Cornell, 2002), utilizing appropriate Engineering Demand Parameters (*EDPs*) to monitor the structure's seismic performance at increasing levels of *IM*. On the above basis, analytical seismic fragility curves were computed, thus forming a key tool for evaluating the structural and

operational integrity of each of the structures of interest as well as for undertaking a probabilistic seismic risk assessment of an oil refinery plant.

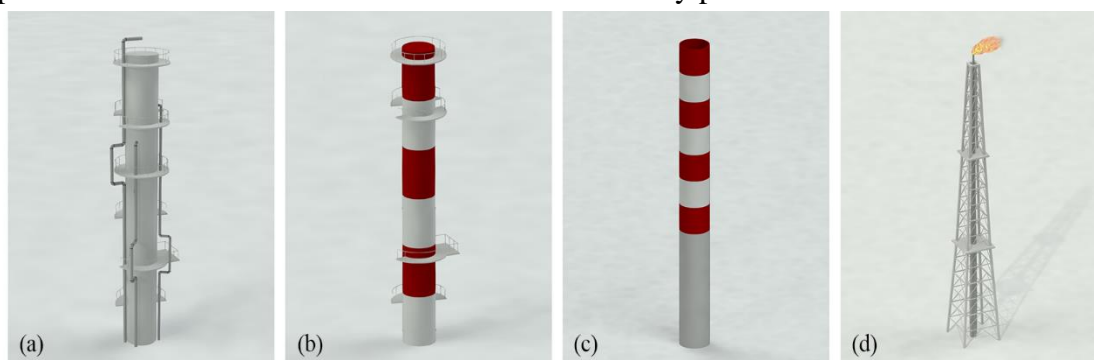


Fig. 1. Schematic illustration of a (a) typical process tower, (b) typical steel chimney, (c) typical RC chimney, (d) typical flare supported by a lattice tower.

2. CASE STUDY DESCRIPTION AND MODELING APPROACH

2.1 Steel process tower

Process towers are considered core oil refinery assets, where various physical and chemical processes take place, e.g., atmospheric distillation, vacuum distillation, polymerization, alkylation and isomerization. (Ancheyta 2011). They are essentially fixed-based freestanding twin-shelled steel structures that form vertical cantilevers, operating under variable pressure and temperature conditions. A schematic illustration of a typical process tower is presented in Fig. 1(a), offering an overview of the structure's typical geometry and main characteristics.

The process tower considered in this study is part of an alkylation unit, where light olefins are combined with isobutane to form high-octane gasoline. The tower is an acid settler, where the hydrocarbons are separated from the free hydrofluoric acid in two parts, operating at different pressure levels but at the same high temperature. For simplicity, the mean value of the operating pressure across the entire height of the structure was considered equal to 0.94MPa to perform the pertinent capacity checks. Past research (Karamanos 1996; Diamanti et al. 2011; Papadaki et al. 2018) suggests that the effect of typical operating pressure on the elastic stiffness of pressure vessels is negligible and was thus disregarded in the structural model developed for estimating the seismic response of the process tower. The tower is 30m high, having an internal diameter equal to 2.6 m. The shell thickness of the tower was defined on the basis of the internal pressure and not its buckling strength. The thickness varies with elevation, resulting in four segments with section thicknesses equal to 16mm (elevations: 0.00 – 14.85m), 18mm (elevations: 14.85 – 23.65m), 19mm (elevations: 23.65 – 26.83m) and 18mm (elevations: 26.83 – 32.73m) from base to top. It should be noted that only the structure's self-weight was accounted for, while the weight of its content was neglected since it is in a vapor state. The total mass of the tower amounts to 49,000kg and it is distributed along its elevation according to its geometrical properties. The base anchorage and the skirt support are assumed to be rugged and not prone to earthquake-induced damage, on account that the base connection components are typically over-designed (see for instance Moharrami and Amini 2014). Thus, uplift, overturning, sliding or excessive deformations of the skirt flange were not considered as possible failure modes in the present study, yet elaborate techniques are available in the literature to account for them (e.g., Cook et al. 2001) if necessary. The reduced-order numerical model that was developed for the process tower (see Fig. 2) consists of several concentrated masses connected through elastic Euler-Bernoulli beam-column elements.

The masses are assigned at different elevations to depict the different courses and the changes in the shell thickness. To undertake all the necessary structural integrity checks at critical locations, such as nozzles and manholes, additional nodes were defined in the model to serve as monitoring points. The stiffness of the beam-column elements was computed based on the diameter and the exterior wall thickness of the tower. Geometrical nonlinearities were also taken into account. The utilized elastic beam-column elements are readily available in the element library of the OpenSees software platform (McKenna and Fenves 2001) that was employed for computing the tower earthquake induced demands.

P- Δ effects were taken into account, while elastic material properties were considered throughout the structure, as there is no ductility in its response. The tower under investigation is constructed from S275 steel grade; an expected mean yield stress of 380MPa was adopted according to Braconi et al. (2013). The modal analysis of the process tower revealed a period of vibration equal to 0.49s for its first two modes (translational in each of the two principal directions) and a third translational mode with a period equal to 0.08s. The Rayleigh damping model was employed, assigning a 2% damping ratio to the 0.49s and 0.08s periods of vibration.

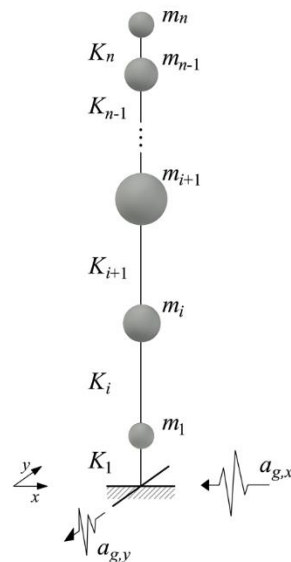


Fig. 2. Generic representation of the lumped mass analytical models that were used for the assessment of the process tower and the chimneys. The stack is discretized in $i = 1, 2, \dots, n$ masses m_i connected with elements of stiffness k_i .

2.2 Steel chimneys

Steel chimneys are tall hollow column structures that are mainly susceptible to damage due to wind hazard. Even though chimneys may be regarded as non-critical structures in an oil refinery, contrary to e.g. the process towers and liquid storage tanks, a potential earthquake-induced failure would result in the disruption of operation across the entire facility. A schematic illustration of a typical steel chimney is depicted in Fig. 1(b) to showcase the generic characteristics and the geometry of such structures.

A relatively short chimney, 30m high, and a taller one, 80m high, were examined. The 30m chimney has an external diameter of 2.2m with its shell thickness being equal to 14mm (elevations: 0.00 – 4.16m) close to its base and 10mm (elevations: 4.16 – 31.20m) at higher elevations. The 80m chimney has six main segments that vary in terms of their external diameter and shell thickness. From bottom to top, the diameter

and thickness of each segment is: 2.5m and 20mm (elevations: 0.00 – 20.00m), 2.5m and 15mm (elevations: 20.00 – 29.00m), 2.35m and 15mm (elevations: 29.00 – 32.00m), 2.2m and 15mm (elevations: 32.00 – 34.00m), 2.2m and 12mm (elevations: 34.00 – 41.80m), 2.2m and 10mm (elevations: 41.80 – 60.00m), and 2.2m and 8mm (elevations: 60.00 – 79.70m).

In both cases, using the model shown in Fig. 2, the masses applied in each one of the defined nodes represent the self-weight of each segment, proportional to its height, diameter, and thickness, accounting also for any attached platforms, ladders, and external coverings. The total mass for the 30m and 80m chimneys are 28,600kg and 101,700kg, respectively. The flue opening located at the base of the chimneys for gas import is typically considered a weak link from a structural point of view and several past studies were devoted to the evaluation of the chimney's stiffness and strength at this particular location (e.g. Huang *et al.* 2004; Gould and Huang 2006). Given the attention paid to this part, in all examined cases the opening is considered to be well-designed and sufficiently strengthened, so as not to affect the chimney's lateral stiffness; hence its potentially adverse effect on the structural integrity was disregarded. The 30m high chimney is made of S275R steel, which has a mean yield stress equal to 397.56MPa per Braconi *et al.* (2013) for steel plate thicknesses in the range of 7mm to 16mm. The 80m high chimney is made of S355R steel grade with a mean yield stress of 487.13MPa (Braconi *et al.* 2013). In a similar manner to the assumptions made for the process tower, uplift, overturning and sliding effects regarding the base anchorage were also neglected for chimneys. For each chimney, a simplified model as per Fig. 2 was developed in the OpenSees analysis platform, using elastic beam-column elements and accounting for P- Δ effects. An initial investigation of the model was undertaken by means of modal analysis to identify the dynamic characteristics of the structures. The analysis resulted in a fundamental translational period of 0.52s for the 30m high chimney and 2.61s for the 80m high chimney in both their principal loading directions. The damping ratio for both chimneys was set equal to 2% in their first and third translational modes of vibration, with the third modes having a period of 0.09s and 0.57s, respectively, for each chimney.

2.3 Reinforced concrete chimney

Concrete is often selected as a construction material for tall industrial chimneys. A schematic illustration of a typical reinforced concrete (RC) chimney that can be found in an oil refinery appears in Fig. 1(c). An 87m tall RC chimney is examined, having an external diameter equal to 4.55m and a shell thickness of 0.3m along its height. The total mass of the chimney is equal to 2,371,000kg. The distribution of the steel reinforcement across the structural height resulted in the RC chimney being partitioned into nine segments, having a longitudinal rebar reinforcement of 94 \emptyset 28 at the lower and 94 \emptyset 12 at the top segment. As expected, the steel reinforcement is lower at higher chimney levels, due to the reduction of the expected internal forces, i.e. the axial and shear forces as well as bending moments. The chimney is made of C30/37 concrete and the rebar reinforcements are of B500C steel grade. The nominal material properties are modified per EN1992-1:2004 (CEN 2004) to obtain the expected values, resulting to an expected concrete mean yield stress equal to $f_{c,m} = 38\text{MPa}$ and steel mean yield stress of $f_{s,m} = 575\text{MPa}$. The flue opening at the base of the chimney is assumed to be stiffened and properly detailed, so as not to affect the lateral stiffness of the chimney at this particular segment, while the base anchorage is considered to be rugged, leading to the neglect of uplift, overturning, and sliding failure mechanisms.

The reduced-order model of the RC chimney was developed following the generic stick model scheme presented in Fig. 2. Contrary to the previously presented structural assets (i.e. steel process tower and steel chimneys), the elements connecting the concentrated masses were defined as nonlinear force-based beam-column fiber section elements, available in the OpenSees element library (McKenna and Fenves 2001). P- Δ effects were also considered. In order to capture material nonlinearity, the Mander *et al.* (1988) stress-strain model was employed, explicitly accounting for the stress-strain behavior of the confined (core) and unconfined (cover) concrete. Cross-section analysis was performed for the concrete sections at the location of the model nodes to assess their moment-curvature capacity. Following a modal analysis, the fundamental period of the RC chimney in both its principal directions was found equal to 1.38s. Since fiber elements were used in the modeling of the chimney, a damping ratio of 1% was assigned to the first and the third overall modes of vibration (Sousa *et al.* 2020), i.e., the first and second translational modes (1.38s and 0.22s) along any of the two principal axes.

2.4 Steel flare

A flare system is an arrangement of piping and specialized equipment that collects hydrocarbon releases from relief valves, blowdown valves, pressure control valves, and manual vents and safely disposes them through combustion at the top of a stack (API 2017) that is called flare stack. The latter can be self-supported, mast-guided, or supported by a lattice tower. Typically, there are a few self-supported flare stacks of relatively short height located within refining units. Contrarily, the main refinery flare is typically located outside the core of the facility for safety reasons and, by virtue of being the tallest, it is often supported by a high-rise lattice tower [see Fig. 1(d)].

A flare tower with a total height of approximately 67.4m was examined. The structure was divided into 12 segments. All structural elements in each segment are made of European steel circular hollow sections (CHS). The lateral stiffness of the tower is controlled by diagonal (truss) members, while the horizontal members form a diaphragm at several elevations. The structure's self-weight was assumed to be concentrated at the four corner joints of each level. The total mass of the tower is equal to 41,700kg. The base anchorage is assumed to be well designed and earthquake-resistant, similar to the previously presented case studies.

A reduced-order numerical model of the flare was developed in OpenSees as illustrated in Fig. 3. The structural members of the lattice tower were modeled with force-based nonlinear beam-column elements and fiber sections. The vertical piping was modeled with elastic beam-column elements and was connected to the supporting lattice tower through the horizontal members that form the diaphragms. P- Δ effects were taken into account. The adopted detailed modeling technique follows the one presented by Billionis and Vamvatsikos (2019) for steel lattice towers. In particular, the stress-strain behavior of the steel fibers was calibrated per each structural member to reproduce their tensile and buckling strength, resulting in curves similar to the one illustrated in Fig. 4. The legs (columns) of the tower were made of S355J2K2 steel grade, which has a mean yield stress f_y equal to 454.90MPa. The rest of the members were made of S235J0JR steel grade having a mean yield stress of 328.80MPa. The steel Young's modulus E was considered equal to 210GPa. To take into account the reduced compression resistance due to the potential flexural buckling of the steel members, the corresponding reduction factor χ was calculated for each circular hollow steel member, according to the procedure prescribed in EN 1993-1-1 (CEN 2005). An example of a stress-strain curve for an indicative section with $\chi = 0.76$ is offered in Fig. 4. This

procedure explicitly accounts for the member slenderness as well as for the cross-section imperfections by means of an imperfection factor that is dependent to the cross-section shape, the fabrication process, and the material type. The fundamental eigenperiod of the flare was found equal to 0.35s in both principal axes. The next translational mode (fourth overall) register at 0.14s. A damping ratio equal to 2% was assigned to its first and fourth overall (or first and second translational for a given axis) modes of vibration (Taillon *et al.* 2012).

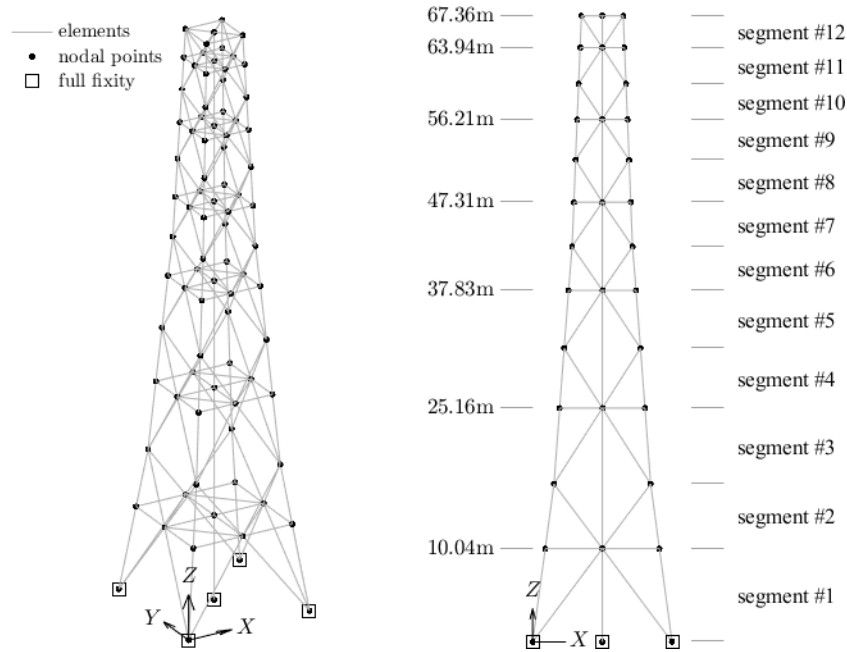


Fig. 3. Flare 3D analysis model in OpenSees.

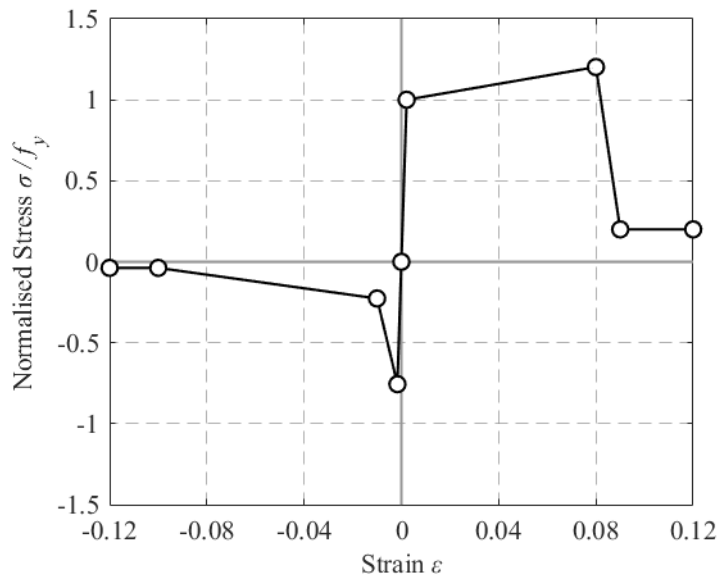


Fig. 4. Steel material stress-strain curve for an indicative flare steel cross-section whose buckling strength is $\chi = 76\%$ times its tensile strength.

A first-mode load pattern was utilized to perform static pushover analysis. The resulting capacity curve is presented in Fig. 5(a), where the base shear V_b is normalized by the tower's total weight W and plotted against the top drift ratio (TDR). Inspecting

the pushover curve suggests that the behavior is mainly elastic with the structure achieving a high strength prior to its yielding point [$V_b/W = 3.12$, $TDR = 0.47\%$, Fig. 5(b)]. Beyond this point, a small increase in terms of top drift leads to failure of the structure in a non-ductile manner [$V_b/W = 3.24$, $TDR = 0.51\%$, Fig. 5(c)]. Therefore, although the strength of the structure is considered to be high, its ductility is limited. Overall, the damage progression depicted by the first-mode pushover curve indicates that the tower's elastic response is followed by a limited plastic region due to the flexural buckling of its diagonal members. Shortly after, this state is followed by the structure's global collapse due to the buckling of its leg members.

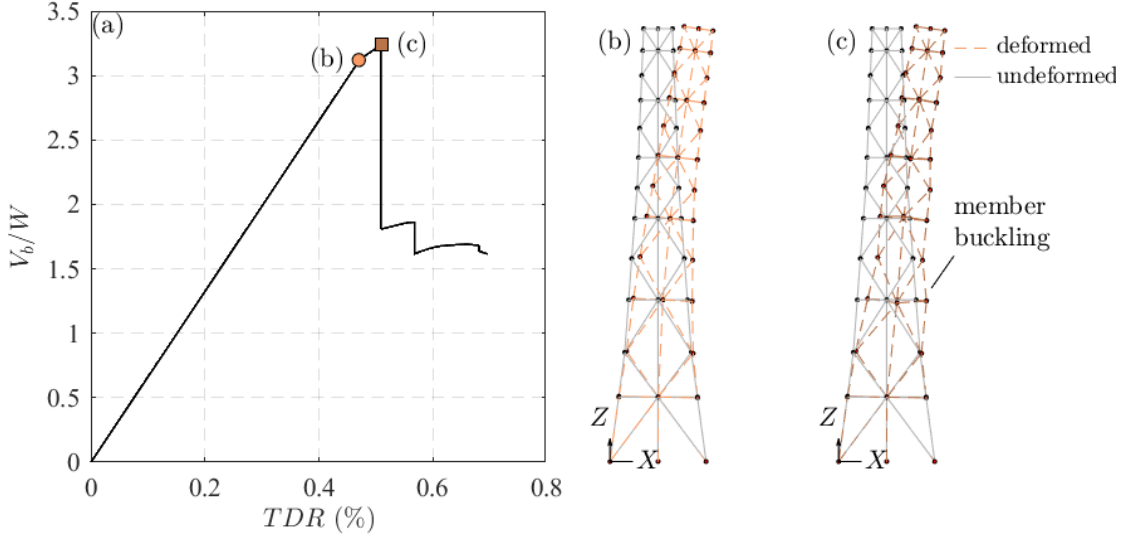


Fig. 5. Flare: (a) Static Pushover analysis curve; illustration of damage progression, featuring (b) yielding and (c) member buckling

3. METHODOLOGY

3.1 Fragility analysis

A reliable, yet resource-efficient, estimation of the seismic fragility is essential for the seismic risk evaluation of the individual structures and consequently the entire facility. The process of deriving analytical fragility curves is well-documented in the international literature (e.g. Dymiotis *et al.* 1999; Kwon and Elnashai 2006; Kazantzi *et al.* 2011; Baker 2015; Bakalis and Vamvatsikos 2018; Silva *et al.* 2014, 2019; Chatzidaki and Vamvatsikos 2021). Seismic fragility is a function of the IM and can be expressed as:

$$F_{LS}(IM) = P[LS \text{ violated} | IM] = P[D > C_{LS} | IM] \quad (1)$$

where $F(\cdot)$ is the cumulative distribution function of its arguments with subscript LS denoting the limit-state of interest; D is the demand, expressed in EDP terms; C_{LS} is the capacity threshold paired to the specific LS and expressed in EDP terms.

Under the typical lognormality assumption (Cornell *et al.* 2002), fragility may be expressed as:

$$P[D > C_{LS} | IM] = \Phi\left(\frac{\ln IM - \ln IM^{LS}}{\beta_{LS}}\right) \quad (2)$$

where IM^{LS} is the median value of the IM required to violate the LS of interest; β_{LS} is the associated lognormal dispersion in the IM , i.e., the standard deviation of the natural logarithm of the data.

3.2 Intensity measures and record selection

The scalar *IM*s adopted are (a) the average spectral acceleration ($AvgS_a$, e.g. Cordova *et al.* 2000; Vamvatsikos and Cornell 2005; Tsantaki and Adam 2013; Eads *et al.* 2015; Kazantzi and Vamvatsikos 2015), being essentially a (moderately) asset-aware *IM*, and (b) the peak ground acceleration (*PGA*), which is deemed to be an asset-agnostic *IM*, as it incorporates no information about the structures investigated. The *PGA* values were computed as the geometric mean of the *PGAs* in the two horizontal orthogonal directions for each one of the considered ground motion records. The $AvgS_a$ values were estimated by taking the geometric mean of spectral ordinates in both principal horizontal directions across a range of equally spaced periods spanning between 0.1s to 1.0s, with an increment of 0.1s. This range of periods was selected to be (approximately) representative of all the structures that are likely to be encountered in an oil refinery plant and not necessarily the most representative for the modal periods of the structures considered in this study. This was a conscious choice, given that the ultimate scope is to develop and showcase a fragility assessment framework that could be readily integrated into an overall oil refinery risk assessment, and hence the range of structural periods should be representative for a large number of structural classes and not limited to those considered herein.

The *IM*s selection is driven by the need to perform risk analysis for multiple structures without introducing unnecessary complexity. In general, one should strive to use the optimal *IM* that best fits each structure, for example emphasizing long periods for a tall stack or short periods for a stiffer pressure vessel. Still, this would enforce the use of event-based probabilistic seismic hazard assessment, also requiring proper correlation relationships among the Ground Motion Prediction Equations (GMPEs) used for each *IM*. In other words, the more *IM*s one introduces, the more cumbersome the overall analysis becomes. On the other end, by adopting a single *IM* that is "good enough" for all structures, one can even use classical Probabilistic Seismic Hazard Analysis (PSHA) results (i.e., a hazard curve) to do the same analysis with much less effort. For this reason, this is a common choice even in urban seismic risk studies (Kohrangi *et al.* 2016, 2021; Silva *et al.* 2019). Thus, *PGA* and $AvgS_a$ were chosen as two useful example cases, since they incorporate accessible *IM* cases easily used in risk analysis studies.

A set of 30 "ordinary" (i.e. non-pulse like, non-long duration) natural ground motion records was selected from the NGA-West2 database (Ancheta *et al.* 2013) for evaluating the induced seismic demands in the structures of interest via IDA, considering the horizontal components of the excitation in both orthogonal directions. The record selection process is documented by Bakalis *et al.* (2018), where the interested reader could find more details on how the hazard-consistent ground motions were selected using the conditional spectrum record selection technique proposed by Kohrangi *et al.* (2017). The record sequence numbers (RSN) of the selected ground motions are provided as follows: 33, 163, 231, 316, 371, 411, 728, 745, 802, 825, 855, 880, 1077, 1177, 1202, 1234, 1259, 1268, 1277, 1503, 1507, 1549, 1596, 1617, 1787, 2654, 2703, 2893, 3222, 3512. It should be noted that the investigated structures were assumed to be located within an oil refinery, extending over an area that is regarded as small enough to neglect any differentiation of ground motion characteristics within the facility boundaries. Therefore, the same ground motion records are applied to all structures, assuming full spatial event-to-event correlation, while record-to-record variability stands as the primary source of uncertainty.

4. DEMAND AND CAPACITY ASSESSMENT

4.1 Steel process tower

The definition of appropriate DSs is required to capture the main failure modes of a structure and consequently quantify its damage in the aftermath of seismic events with various intensities. Two distinct mutually exclusive DSs (i.e. DS1 and DS2) were defined for the process tower and paired to damage levels that are likely to undermine its operational and structural integrity.

The transition to the less severe DS1 is signified upon the exceedance of the 0.5% *TDR* threshold, which essentially corresponds to the damage limitation threshold of the EN1998-6:2005 (CEN 2005) provisions. Higher top displacements are deemed to result in the disruption of the tower operation by damaging the attached piping. One may introduce further damage states for piping at higher levels of interstory drift or, e.g., excessive rotation at the pipe attachment (Corritore et al. 2021). Still, pertinent data is lacking in general and largely depends on the pipe and on the pipe-vessel connection characteristics. Therefore, we focused only on the onset of damage. On the other hand, DS2 is associated with the structural integrity of the tower, and the transition to this DS was checked against a shell buckling verification criterion adopted by EN1993-1-6:2007 (CEN 2007). To assess the local stability of the shell, the required axial and shear forces, as well as the bending moments were obtained along the tower elevation at each analysis step of the response history analyses. The tower was treated as a stepped cylinder according to EN1993-1-6:2007. Different segments of the tower with equal wall thickness were uniformly treated, essentially resulting in a three-segment stepped cylinder as per Annex D of EN1993-1-6:2007. The buckling strength verification is performed through the variable R_c defined as:

$$R_c = \left(\frac{\sigma_E}{\sigma_R} \right)^{k_x} + \left(\frac{\tau_E}{\tau_R} \right)^{k_\tau}, \quad (3)$$

where σ_E is the axial buckling stress; σ_R is the axial buckling resistance; τ_E is the shear buckling stress; τ_R is the shear buckling resistance; and k_x, k_τ are the combination factors for the interaction of axial compression and shear. The peak value of R_c is computed at each time step to account for the interaction of meridional (axial) compression with the coexistent shear and internal pressure. The DS description and the corresponding capacity thresholds are summarized in Table 1. When R_c exceeds unity, failure is encountered, or strictly speaking, transition to DS2 is observed, deemed to be representative of structural integrity loss.

Table 1. Process Tower: DS classification and capacity thresholds.

Damage States	Description	Capacity Checks
DS1	Top drift of the tower causing disruption of the operation or damage to the connected piping	$TDR \geq 0.5\%$
DS2	Local buckling of the shell causing severe structural damage	$R_c \geq 1.0$

The 16/50/84% fractile IDA curves for the process tower are presented in Fig. 6, where the *EDP*s related to the DSs are plotted against the two considered *IM*s. As stated earlier, the *EDP* estimates are derived from an elastic model (in terms of the material properties), therefore the response is linear for DS1 [see Fig. 6(a-b)]. By virtue of R_c being a nonlinear combination of the model outputs, the IDA curves shown in Fig. 6(c-

d) are actually nonlinear, yet this nonlinearity is not that apparent for the presented range of intensities.

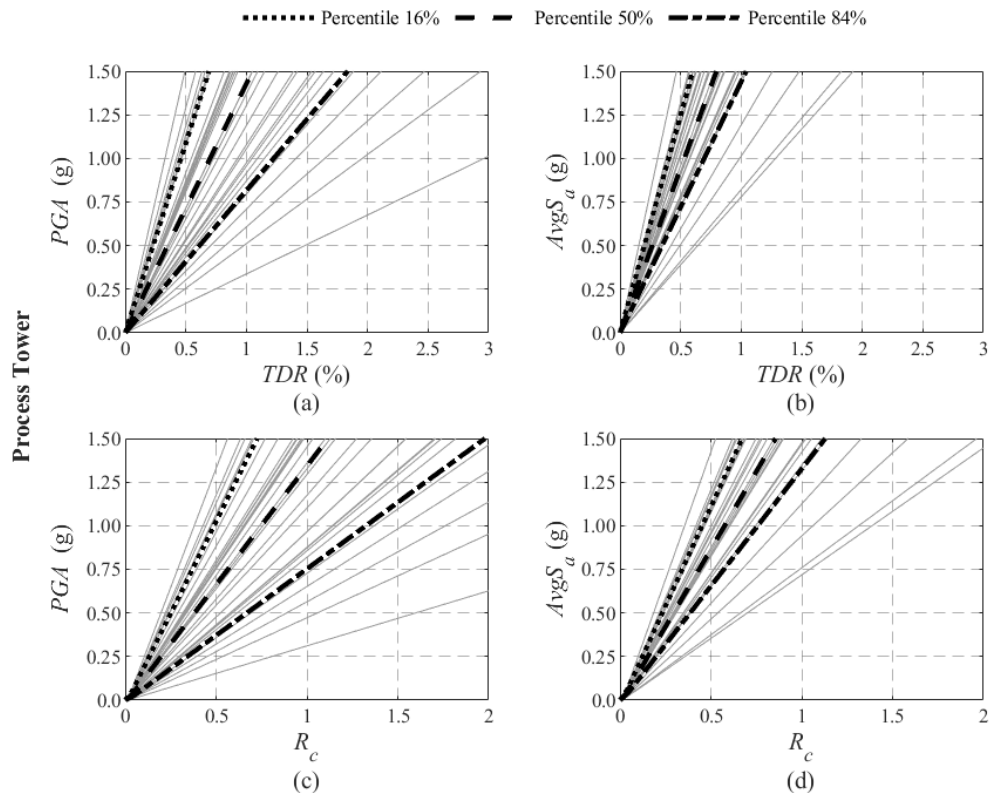


Fig. 6. Process tower IDA curves and 16/50/84% fractiles: (a) TDR versus PGA , (b) TDR versus $AvgS_a$, (c) R_c versus PGA , (d) R_c versus $AvgS_a$.

4.2 Steel chimneys

Three distinct DSs were considered for the performance assessment of the steel chimneys. DS1 is related to their operability and the corresponding 0.5% limit for the TDR of the chimneys is adopted after EN1998-6:2005. DS2 is associated with liner damage and transition to this state was considered to occur at an Intersegment Drift Ratio (IDR , namely the drift angle between two consecutive levels of the chimney) of 1.2% after the EN1998-6:2005 provisions. Finally, the transition to DS3 signals the structural failure of the chimney due to the local buckling of its outer shell. The latter was checked following the same procedure outlined in Section 4.1 for the process tower according to EN1993-1-6:2007. A stepped cylinder approach was employed and the sequential segments with the same wall thickness were treated as one. The checks were performed considering the peak parameter R_c [after Eq. (3)] as the EDP . The description of the steel chimney DSs and their pertinent capacity thresholds are listed in Table 2.

Table 2. Steel Chimneys: DS classification and capacity thresholds.

Damage States	Description	Capacity Checks
DS1	Top drift of the chimney causing damage to the connected piping	$TDR \geq 0.5\%$
DS2	Intersegment drift causing damage to the liner	$IDR \geq 1.2\%$
DS3	Local buckling of the shell causing severe structural damage	$R_c \geq 1.0$

The IDA results are presented in Fig. 7 and Fig. 8 for the 30m and 80m high steel chimneys, respectively. As Fig. 7(a-d) attest, the linear model displays a response of high variability that could be partially attributed to the higher mode effects. The IDA curves presented in Fig. 7(e-f) deviate from linearity, an effect of the R_c criterion being a nonlinear function of the otherwise linear model. The same observations hold for the IDA curves of the 80m high steel chimney that appear in Fig. 8.

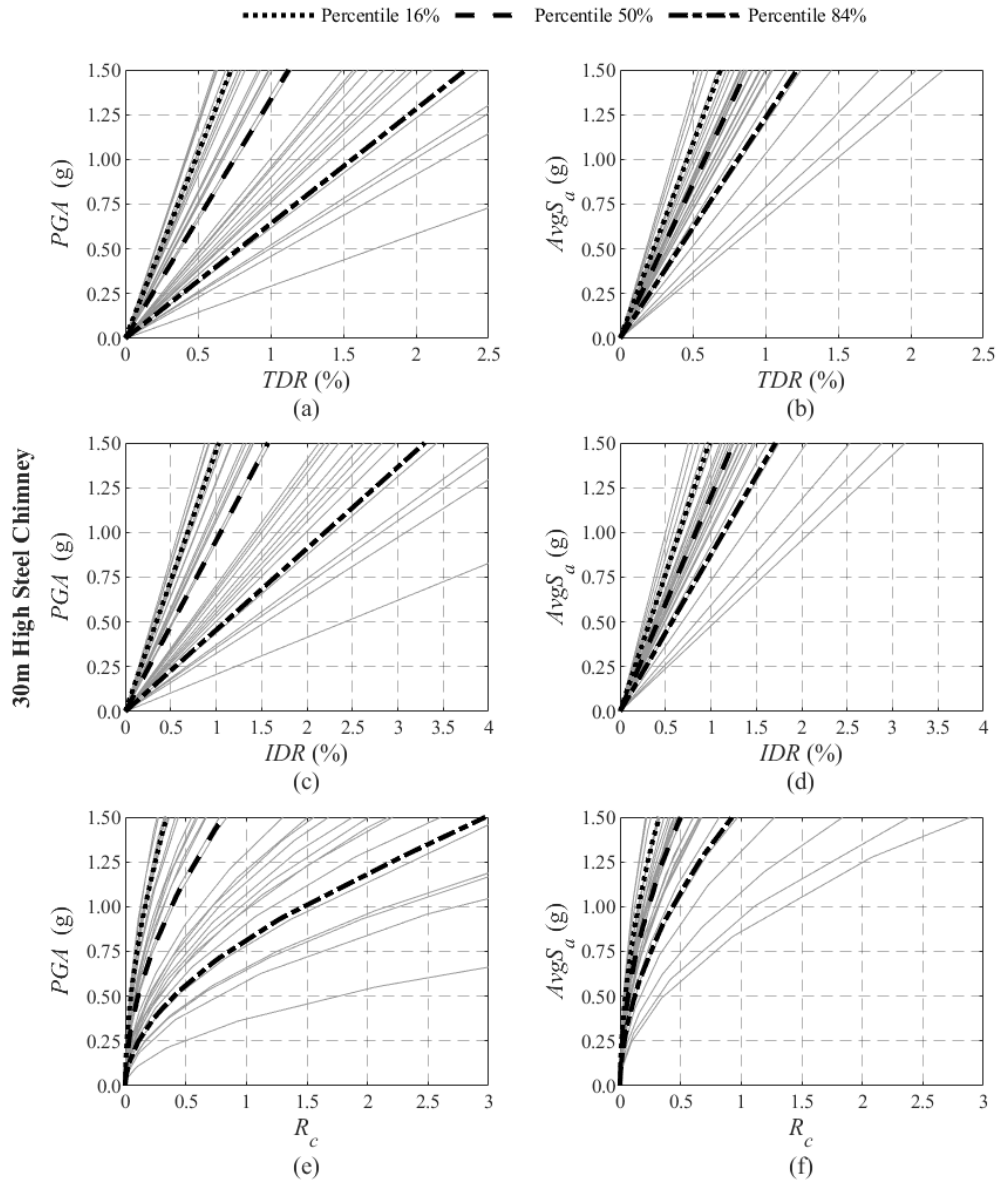


Fig. 7. 30m steel chimney IDA curves and 16/50/84% fractiles: (a) TDR versus PGA , (b) TDR versus $AvgS_a$, (c) IDR versus PGA , (d) IDR versus $AvgS_a$, (e) R_c versus PGA , (f) R_c versus $AvgS_a$.

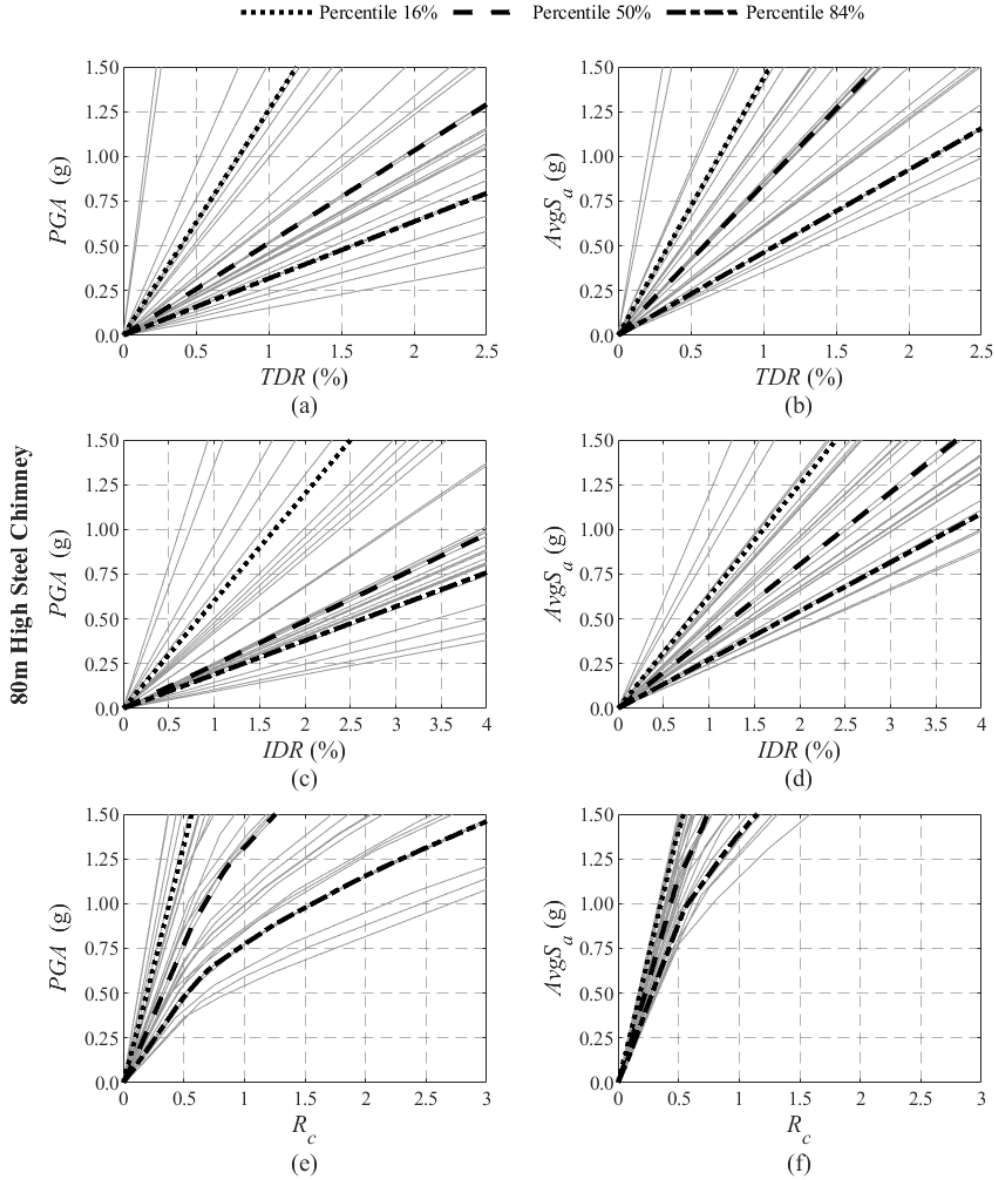


Fig. 8. 80m steel chimney IDA curves and 16/50/84% fractiles: (a) TDR versus PGA , (b) TDR versus $AvgS_a$, (c) IDR versus PGA , (d) IDR versus $AvgS_a$, (e) R_c versus PGA , (f) R_c versus $AvgS_a$.

4.3 Reinforced concrete chimney

Three DSs were considered for the RC chimney. DS1 is attained at a TDR equal to 0.5% similarly to the steel chimneys. DS2 was associated with two failure modes, one related to liner damage that was assumed to occur at IDR demand exceeding 1.2% and a second one related to the transition of the cross-sections to their yielding state that could be paired with low to moderate structural damages (e.g. visible cracking). For the latter failure mode, the check was performed along the chimney elevation by checking at each analysis time-step whether the seismic demand, expressed in terms of the section bending moment (M_E), exceeds the yield moment (M_y) capacity of the pertinent cross-section. The transition to DS2 is signaled by either of those checks being violated. It should be noted that DS2 is paired with low to moderate structural damage that would however require the shutdown of the chimney and the execution of extensive repair

works. The scalar parameter R_2 , defined as the maximum of two demand-to-capacity ratios to account for both of the aforementioned damage states, was the *EDP* considered for DS2:

$$R_2 = \max \left\{ \frac{M_E}{M_y} ; \frac{IDR(\%)}{1.2\%} \right\} \quad (4)$$

where, M_E is the seismic demand in terms of bending moment; IDR is the intersegment drift (in %); M_y is the yield moment.

DS3 is related to severe structural damage of the RC shell (global failure of the structure). The attainment of DS3 is signified when the bending moment at the cross-section (M_E) exceeds its ultimate bending moment capacity (M_u). The R_3 demand-to-capacity ratio was employed as the *EDP* for DS3:

$$R_3 = \frac{M_E}{M_u} \quad (5)$$

The description of the DSs along with their thresholds are listed in Table 3. Fig. 9 presents the IDA curves obtained for the reinforced concrete chimney. The waving IDA curves illustrated reveal the notable nonlinear response of the RC chimney.

Table 3. RC Chimney: DS classification and capacity.

Limit States	Description	Capacity Checks
DS1	Top drift of the chimney causing damage to the connected piping	$TDR \geq 0.5\%$
DS2	Intersegment drift causing damage to the liner OR cross-section yielding causing low-to-moderate structural damage (e.g. cracking)	$R_2 \geq 1.0$
DS3	Cross-section failure due to exceedance of ultimate bending moment causing severe structural damage	$R_3 \geq 1.0$

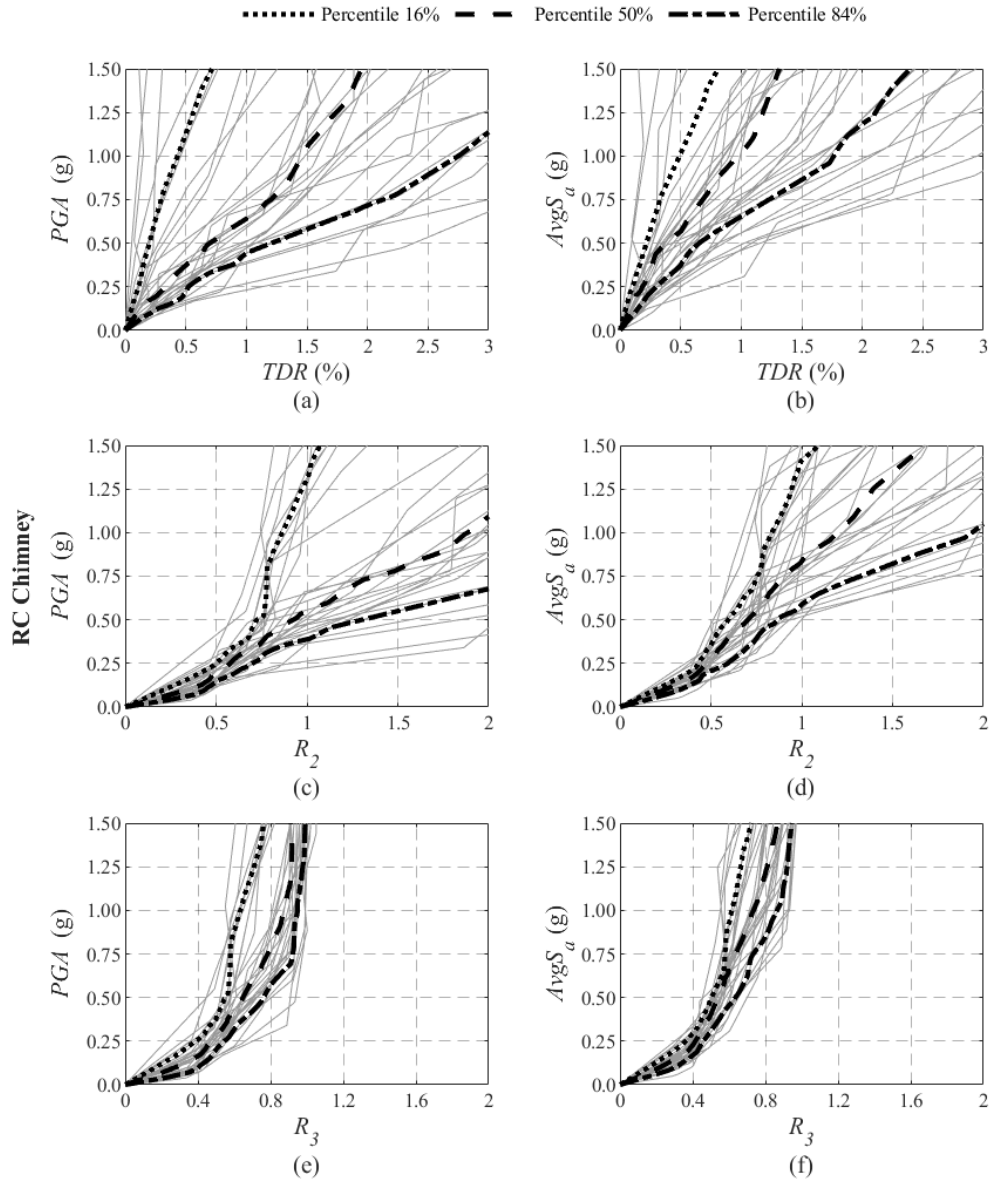


Fig. 9. RC Chimney IDA curves and 16/50/84 fractiles: (a) TDR versus PGA , (b) TDR versus $AvgS_a$, (c) R_2 versus PGA , (d) R_2 versus $AvgS_a$, (e) R_3 versus PGA , (f) R_3 versus $AvgS_a$.

4.4 Steel flare

Three DSs were defined for the flare. In particular, DS1 is related to operational disturbances, where the 0.5% limit for TDR after EN1998-6:2005 was adopted as a threshold to prevent damage to the attached mechanical equipment. DS2 is associated with nonstructural damage in the vertical piping. Thus, the intersegment drift that might cause damage to the vertical piping is checked against the 1.2% limit of EN1998-6:2005. Transition to DS3, deemed to be the global collapse damage state, is signaled by the failure of a member of the tower either in tension or compression (member global buckling). Based on the pushover findings (Fig. 5), the failure of a single member is considered herein to lead to the global instability for the entire tower. Therefore, the integrity of all structural member was checked, and in particular of the legs and diagonal members that are the main load bearing elements. To this end, the parameter R_M was

introduced as the maximum demand-to-capacity ratio of tensile or axial failure over all legs and diagonals to identify the most critical failure mode:

$$R_M = \max_{\text{all } i} \left\{ \max \left(\frac{N_{E,t}^i}{N_{y,t}^i}; \frac{N_{E,c}^i}{N_{y,c}^i} \right) \right\} \quad (6)$$

where for each member (leg or diagonal) i : $N_{E,t}^i$ is the tensile axial force demand; $N_{y,t}^i$ is the tensile axial resistance; $N_{E,c}^i$ is the compressive axial force demand; $N_{y,c}^i$ is the buckling resistance. It should be noted that some bending moment develops in the tower legs; however, this parasitic moment was found to be very low for such a triangulated lattice tower and was thus neglected. Consequently, the integrity of the members was checked solely on the basis of the developed axial forces. The description of the DSs and the corresponding capacity thresholds are tabulated in Table 4.

Table 4. Flare: DS classification and capacity thresholds.

Damage States	Description	Capacity checks
DS1	Top drift of the tower causing damage to mechanical equipment	$TDR \geq 0.5\%$
DS2	Intersegment drift causing damage to the vertical piping	$IDR \geq 1.2\%$
DS3	Member tensile or buckling failure causing global collapse	$R_M \geq 1.0$

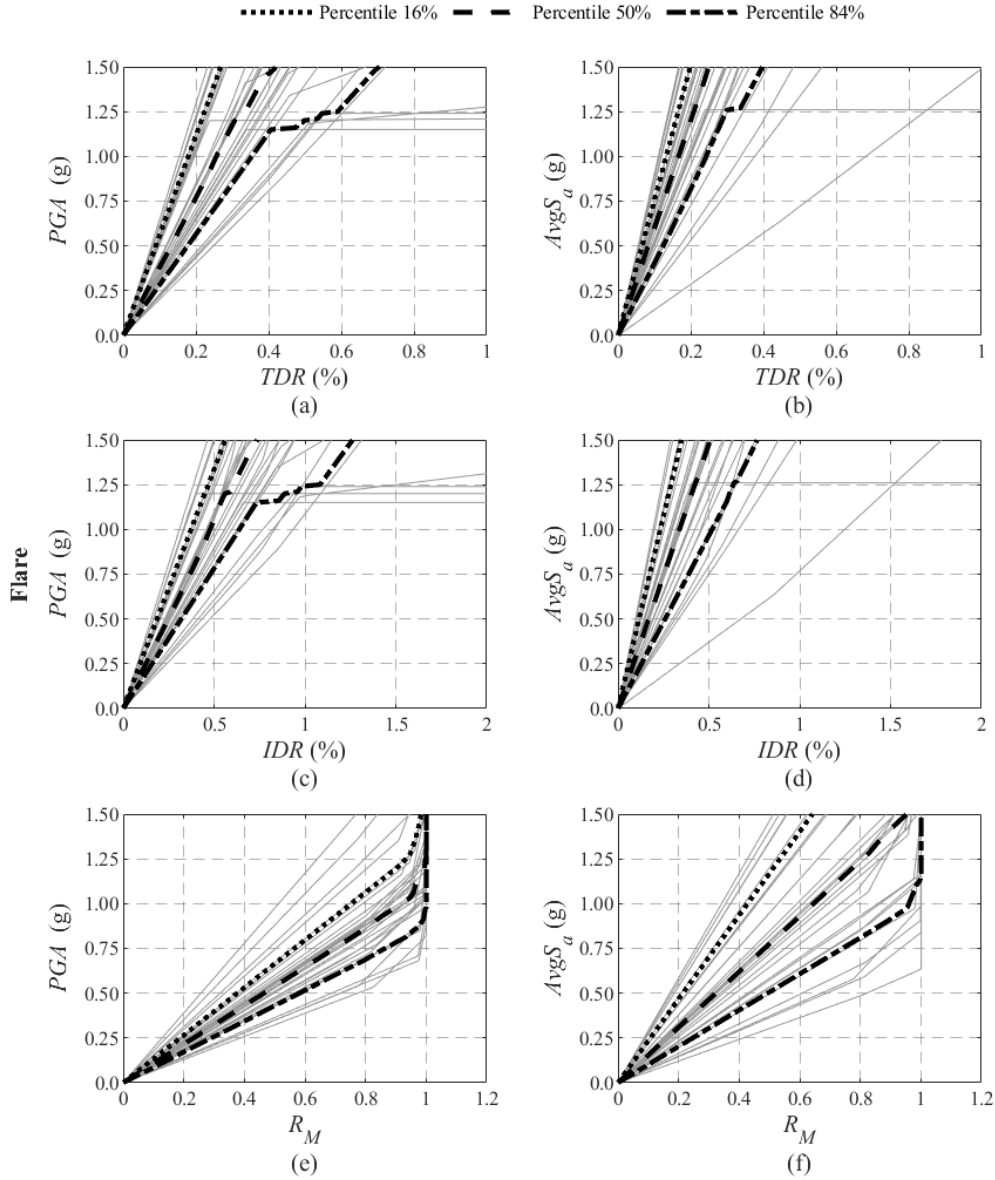


Fig. 10. Flare IDA curves and 16/50/84% fractiles: (a) TDR versus PGA , (b) TDR versus $AvgS_a$, (c) IDR versus PGA , (d) IDR versus $AvgS_a$, (e) R_M versus PGA , (f) R_M versus $AvgS_a$.

The IDA curves for the flare are presented in Fig. 10 for both IMs and the three $EDPs$ considered for each one of the defined DSs . As can be inferred, especially by inspecting the strength-limited R_M results, the structural behavior is elastic up to a critical point, beyond which failure occurs without allowing any significant ductility to develop in the model.

5. FRAGILITY CURVES

Fragility curves were generated for each DS , employing a lognormal distribution fitting on the empirical data points. Median and dispersion estimates are tabulated in Table 5 for each one of the structures examined. To account for the capacity-related uncertainties in the fragility definition, 100 normally distributed capacity realizations were generated for each ground motion record, assuming a 20% covariance (COV)

around the median DS threshold capacities without any correlation among different failure modes defining a given DS. Fig. 11 presents the empirical cumulative distribution function (CDF) data points along with the associated lognormal fits.

The results for the process tower, shown in Fig. 11(a-b), indicate that (a) the lognormal distribution is a good approximation of the process tower seismic fragility; (b) there would not be a high probability of damage for the process tower for low to moderate intensity earthquakes; and (c) for seismic events of higher intensity, the probability for the structure to lose its operational capacity is high, while that of losing its structural integrity is lower but still nonnegligible. Another notable observation is that the dispersion of the seismic fragility at both DSs is lower when $AvgS_a$ is considered. This means that the average spectral acceleration, as defined in this study, is a more efficient *IM* than the *PGA* across the entire structural response of interest, and hence one needs to invest less computational effort for delivering robust response estimates by means of response history analyses if such an *IM* is adopted (Kazantzi and Vamvatsikos, 2015).

With regards to the steel chimneys, as can be inferred by inspecting Fig. 11(c-d) for the 30m chimney and Fig. 11(e-f) for the 80m chimney, regardless of the chimney height, the DSs are sequential, while the tallest chimney is in general more susceptible to both non-structural and structural damages compared to the shorter 30m high chimney. With reference to the 80m high chimney, DS1 and DS2 fragility curves are very close to each other [see Fig. 11(e-f)]. This condition essentially implies that its operational integrity is likely to be undermined by either excessive top displacements or damage imposed to its liner. A comparison between the two steel chimneys reveals that the 80m high chimney is more susceptible to reaching the DS1 and DS2 compared to the 30m high chimney, and also slightly more prone to local buckling (i.e. DS3, in terms of the fragility curves with *PGA* as an *IM*). The two chimneys having comparable fragility to local buckling may be attributed to the higher steel grade used for the taller one, as well as to the contribution of the higher eigenmodes in the response. Moreover, the 80m high steel chimney is in fact a very flexible structure, a condition that actually results in the reduction of shear forces and moments during the seismic response.

The fragility curves for the RC chimney [Fig. 11(g-h)] reveal that the chimney has a low probability of reaching DS3 and consequently being severely damaged, but is much more susceptible to nonstructural damages or other minor damages (associated with the attainment of DS1 and DS2). This could undermine its operational capacity and result in severe downtime for repairs something that should certainly be accounted for in a broader risk assessment process.

For the flare asset, a notable observation with reference the computed fragility curves [Fig. 11(i-j)] is that DS3, which signals the violation of the structural integrity of the lattice tower, is the most critical DS, with the highest probability of exceedance among the other DSs, across the entire range of intensity levels. This observation could be explained on account of the pushover findings (see Fig. 8), illustrating that the drift limits specified in the code (and adopted herein as the DS1/2 thresholds, see Table 4) cannot be easily reached by this stiff lattice tower, at least not before a member buckles first. Nevertheless, the overall seismic performance of the examined flare is deemed to be satisfactory, since substantially high intensity levels are needed to impose the seismic demands that could trigger a catastrophic failure. Quite notably also, the *PGA* fragility estimates are characterized by slightly lower dispersion values compared to those obtained on the basis of $AvgS_a$. This is a byproduct of the conscious decision to

evaluate the $AvgS_a$ across a range of periods (0.1 – 1.0s) that are mostly longer than the 0.35s fundamental period of the stiff flare.

Table 5. Median and dispersion of fragility curves (lognormal distribution fitting) for each of five structures.

Damage States		DS1		DS2		DS3	
		median (g)	dispersion	median (g)	dispersion	median (g)	dispersion
Process Tower	<i>PGA</i>	0.65	0.54	1.16	0.54	—	—
	<i>AvgS_a</i>	0.91	0.39	1.63	0.39	—	—
30m Steel Chimney	<i>PGA</i>	0.57	0.59	0.93	0.59	1.45	0.56
	<i>AvgS_a</i>	0.80	0.39	1.31	0.39	2.03	0.35
80m Steel Chimney	<i>PGA</i>	0.31	0.88	0.35	0.71	1.34	0.58
	<i>AvgS_a</i>	0.43	0.65	0.50	0.46	1.87	0.29
RC Chimney	<i>PGA</i>	0.37	0.89	0.62	0.69	1.83	1.00
	<i>AvgS_a</i>	0.60	0.55	0.87	0.52	2.43	0.88
Flare	<i>PGA</i>	1.78	0.41	2.22	0.55	1.08	0.34
	<i>AvgS_a</i>	2.49	0.47	3.11	0.56	1.51	0.46

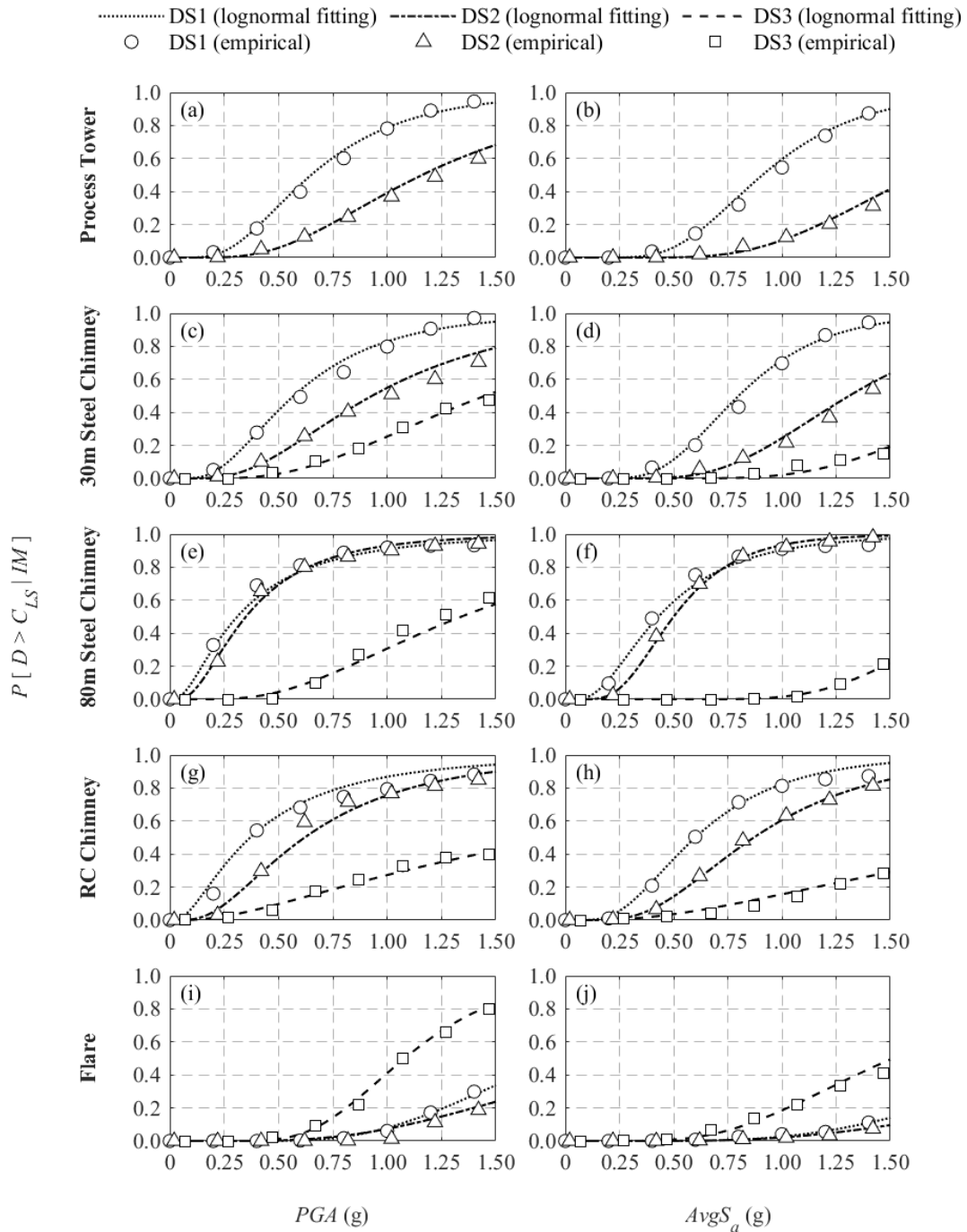


Fig. 11. Fragility curves using as IM the PGA (left) and the $AvgS_a$ (right) for each of five structures.

6. CONCLUSIONS

A comprehensive analytical seismic fragility assessment for high-rise structures encountered in oil refineries was presented. Four typical structural typologies were examined, namely a process tower, two steel chimneys, a reinforced concrete chimney, and a flare. A set of numerical models was developed, on a minimum needed complexity basis, to ensure that the dominant failure modes are always captured while the framework remains efficient for practical applications, by directing the

computational power and skill resources where needed most. To assess the seismic demands across a range of *IM* levels, IDAs were performed using a set of hazard-consistent ground motion records. Appropriate damage states were defined to account for both the serviceability and the structural integrity of the considered assets. High-quality analytical fragility curves were derived that account for both the epistemic uncertainties associated with the structural capacity and the randomness stemming from the ground motion record characteristics. It was demonstrated that the examined structures can suffer significant structural damage or collapse only at very high levels of seismic intensity. On the other hand, relatively lower accelerations may disrupt their operation and consequently affect the functionality of the entire oil refinery. For instance, failure of the connected piping would require the shut-down of an entire refinery unit for undertaking the needed repairs. The presented results showcased that seismic hazard should explicitly be considered when assessing, not only the structural, but also the operational integrity of individual structures that form an integrated critical industrial facility. The produced analytical seismic fragility curves along with the presented methodology can be exploited by researchers, engineers, and stakeholders to conduct a seismic risk assessment of an entire oil refinery unit.

ACKNOWLEDGEMENTS

The authors would like to thank Ms. E. Vourlakou for preparing the photorealistic images of the buildings.

REFERENCES

- API (American Petroleum Institute). 2017. *ANSI/API STD 537 Flare details for petroleum, petrochemical, and natural gas industries*. 3rd edition. Washington, DC, USA: API.
- Ancheta T, Darragh R, Stewart J, et al (2013) PEER NGA-West2 Database, Technical Report PEER 2013/03. Pacific Earthquake Engineering Research Center, Berkeley, CA
- Ancheyta, J. 2011. *Modeling and simulation of catalytic reactors for petroleum refining*. New Jersey, NJ, USA: Wiley & Sons, Inc. <https://doi.org/10.1002/9780470933565>
- ASCE/SEI. 2017. *Minimum design loads and associated criteria for buildings and other structures, ASCE/SEI 7-16*. Reston, VA, USA: Structural Engineering Institute of American Society of Civil Engineers. <https://doi.org/10.1061/9780784414248>
- Bakalis, K., and S. A. Karamanos. 2021. "Uplift mechanics of unanchored liquid storage tanks subjected to lateral earthquake loading." *Thin-Walled Structures*, 158: 107145. <https://doi.org/10.1016/j.tws.2020.107145>
- Bakalis, K., M. Kohrangi, and D. Vamvatsikos. 2018. "Seismic intensity measures for above-ground liquid storage tanks." *Earthquake Engineering & Structural Dynamics*, 47 (9): 1844–1863. <https://doi.org/10.1002/eqe.3043>
- Bakalis, K., D. Vamvatsikos, and M. Fragiadakis. 2017. "Seismic risk assessment of liquid storage tanks via a nonlinear surrogate model." *Earthquake Engineering & Structural Dynamics*, 46 (15): 2851–2868. <https://doi.org/10.1002/eqe.2939>

- Bakalis, K., and D. Vamvatsikos. 2018. "Seismic fragility functions via nonlinear response history analysis." *Journal of Structural Engineering (ASCE)*, 144 (10): 04018181. [https://doi.org/10.1061/\(ASCE\)ST.1943-541X.0002141](https://doi.org/10.1061/(ASCE)ST.1943-541X.0002141)
- Baker, J.W. 2015. "Efficient analytical fragility function fitting using dynamic structural analysis." *Earthquake Spectra*, 31(1): 579–599. <https://doi.org/10.1193/021113EQS025M>
- Bi, S., A. Kiaghadi, B. C. Schulze, C. Bernier, P. B. Bedient, J. E. Padgett, H. Rifai, and R.J. Griffin. 2021. "Simulation of potential formation of atmospheric pollution from aboveground storage tank leakage after severe storms." *Atmospheric Environment*, 248: 118225. <https://doi.org/10.1016/j.atmosenv.2021.118225>
- Bilionis, D. V., and D. Vamvatsikos. 2017. "Wind performance assessment of telecommunication towers: a case study in Greece." In *Proc., 7th Interactional Conference on Computational Methods in Structural Dynamics and Earthquake Engineering (COMPDYN 2017)*, 5741–5755. Crete Island, Greece. <https://doi.org/10.7712/120119.7342.19629>
- Braconi, A., Finetto, M., Degee, H., Hausoul, N., et al., 2013. "Optimising the seismic performance of steel and steel-concrete structures by standardising material quality control (OPUS)", European Commission, Directorate-General for Research and Innovation, Publications Office. <https://doi.org/10.2777/79330>
- Bursi, O. S., R. Di Filippo, V. La Salandra, M. Pedot, and M. S. Reza. 2018. "Probabilistic seismic analysis of an LNG subplant." *Journal of Loss Prevention in the Process Industries*, 53: 45–60. <https://doi.org/10.1016/j.jlp.2017.10.009>
- CEN. 2004. *Eurocode 8: Design of structures for earthquake resistance. Part 1: General rules, seismic actions and rules for buildings. EN1998-1*. Brussels: European Committee for Standardization (CEN). <https://eurocodes.jrc.ec.europa.eu/showpage.php?id=138>
- CEN 2005. *Eurocode 1: Actions on structures - Part 1-1: General actions - Densities, self-weight, imposed loads for buildings. EN1991-1-1*. Brussels: European Committee for Standardization (CEN). <https://eurocodes.jrc.ec.europa.eu/showpage.php?id=130>
- CEN. 2005. *Eurocode 3 - Design of steel structures - Part 1-6: Strength and stability of shell structures. EN 1993-1-6*. Brussels: European Committee for Standardization (CEN). <https://eurocodes.jrc.ec.europa.eu/showpage.php?id=133>
- Chatzidaki, A., & Vamvatsikos, D. 2021. "Mixed probabilistic seismic demand models for fragility assessment." *Bulletin of Earthquake Engineering*, 19(15), 6397-6421. <https://doi.org/10.1007/s10518-021-01163-4>
- Cook, R. A., Bobo, B. J., and Ansley, M. H. (2001). Design Guidelines for Annular Base Plate, Structures Research Report N 716. Gainesville, Florida: Department of Civil and Coastal Engineering, University of Florida
- Cordova, P. P., G. G. Deierlein, S. S. Mehanny, and C. A. Cornell. 2000. "Development of a two-parameter seismic intensity measure and probabilistic assessment procedure." In *Proc., 2nd US–Japan Workshop on Performance-based Earthquake Engineering Methodology for RC Building Structures*. Sapporo, Hokkaido, Japan.

- Cornell, C. A., F. Jalayer, R. O. Hamburger, and D. A. Foutch. 2002. "The probabilistic basis for the 2000 SAC/FEMA steel moment frame guidelines." *Journal of Structural Engineering (ASCE)*, 128 (4): 526–533. [https://doi.org/10.1061/\(ASCE\)0733-9445\(2002\)128:4\(526\)](https://doi.org/10.1061/(ASCE)0733-9445(2002)128:4(526))
- Corritore D., Paolacci F., Caprinuzzi S. 2021. "A screening methodology for the identification of critical units in major-hazard facilities under seismic loading." *Frontiers in built environment*: (7): 780719. <https://doi.org/10.3389/fbuil.2021.780719>
- Diamanti, K., Doukas, I., & Karamanos, S. A. 2011. "Seismic analysis and design of industrial pressure vessels." In *III ECCOMAS Thematic Conf. on Computational Methods in Structural Dynamics and Earthquake Engineering, COMPDYN*, Corfu, Greece.
- Di Sarno, L., and G. Karagiannakis. 2021. "Seismic performance-based assessment of a RC pipe rack accounting for dynamic interaction." *Structures*, 33: 4604–4615. <https://doi.org/10.1016/j.istruc.2021.07.031>
- Dymiotis, C., A. J. Kappos, and M. K. Chryssanthopoulos. 1999. "Seismic reliability of RC frames with uncertain drift and member capacity." *Journal of Structural Engineering (ASCE)*, 125 (9): 1038–1047. [https://doi.org/10.1061/\(ASCE\)0733-9445\(1999\)125:9\(1038\)](https://doi.org/10.1061/(ASCE)0733-9445(1999)125:9(1038))
- Eads, L., E. Miranda, and D. G. Lignos. 2015. "Average spectral acceleration as an intensity measure for collapse risk assessment." *Earthquake Engineering & Structural Dynamics*, 44 (12): 2057–2073. <https://doi.org/10.1002/eqe.2575>
- Farhan, M., and S. Bousias. 2020. "Seismic fragility analysis of LNG sub-plant accounting for component dynamic interaction." *Bulletin of Earthquake Engineering*, 18: 5063–5085. <https://doi.org/10.1007/s10518-020-00896-y>
- Girgin, S. 2011. "The natech events during the 17 August 1999 Kocaeli earthquake: aftermath and lessons learned." *Natural Hazards and Earth System Sciences*, 11 (4): 1129–1140. <https://doi.org/10.5194/nhess-11-1129-2011>
- Godoy, L. A. 2007. "Performance of storage tanks in oil facilities damaged by hurricanes Katrina and Rita." *Journal of Performance of Constructed Facilities (ASCE)*, 21 (6): 441–449. [https://doi.org/10.1061/\(ASCE\)0887-3828\(2007\)21:6\(441\)](https://doi.org/10.1061/(ASCE)0887-3828(2007)21:6(441))
- Gould, P. L., and W. Huang. 2006. "Higher mode effects in the nonlinear static analysis of a collapsed chimney." In *Proc., Structures Congress 2006: Structural Engineering and Public Safety*, St. Louis, MO, USA. [https://doi.org/10.1061/40889\(201\)19](https://doi.org/10.1061/40889(201)19)
- Guo, X., and C. Zhang. 2019. "Seismic fragility analysis of corroded chimney structures." *Journal of Performance of Constructed Facilities (ASCE)*, 33 (1): 04018087. [https://doi.org/10.1061/\(ASCE\)CF.1943-5509.0001241](https://doi.org/10.1061/(ASCE)CF.1943-5509.0001241)
- Guo, X., W. Chen, and J. Yu. 2018. "Combined effect of vertical and horizontal ground motions on failure probability of RC chimneys." *Advances in Civil Engineering*, 9327403. <https://doi.org/10.1155/2018/9327403>
- Hatayama, K. 2015. "Damage to oil storage tanks from the 2011 Mw 9.0 Tohoku-Oki tsunami." *Earthquake Spectra*, 31 (2): 1103–1124. <https://doi.org/10.1193/050713EQS120M>
- Hatayama, K. 2008. "Lessons from the 2003 Tokachi-oki, Japan, earthquake for prediction of long-period strong ground motions and sloshing damage to oil

- storage tanks.” *Journal of Seismology*, 12: 255–263. <https://doi.org/10.1007/s10950-007-9066-y>
- Huang, W., P. L. Gould, R. Martinez, G. S. Johnson. 2004. “Non-linear analysis of a collapsed reinforced concrete chimney.” *Earthquake Engineering & Structural Dynamics*, 33: 485–498. <https://doi.org/10.1002/eqe.362>
- Karamanos, S.A. 1996. “Stability of pressurized long inelastic cylinders under radial transverse loads.” *Computational Mechanics* 18, 444–453. <https://doi.org/10.1007/BF00350252>
- Karakostas, C. Z., I. F. Moschonas, V. A. Lekidis, and S. P. Papadopoulos. 2015. “Seismic performance of industrial pressure vessels: Parametric investigation of simplified modeling approaches for vulnerability assessment.” In *Proc., 5th International Conference on Computational Methods in Structural Dynamics and Earthquake Engineering (COMPDYN 2015)*, 2021–2037. Crete Island, Greece. <https://doi.org/10.7712/120115.3520.944>
- Kazantzi, A. K., T. D. Righiniotis, and M. K. Chryssanthopoulos. 2011. “A simplified fragility methodology for regular steel MRFs.” *Journal of Earthquake Engineering*, 15 (3): 390–403. <https://doi.org/10.1080/13632469.2010.498559>
- Kazantzi, A. K., and D. Vamvatsikos. 2015. Intensity measure selection for vulnerability studies of building classes. *Earthquake Engineering & Structural Dynamics*, 44(15): 2677–2694. <https://doi.org/10.1002/eqe.2603>
- Kohrangi, M., Bazzurro, P., & Vamvatsikos, D. 2021. “Seismic risk and loss estimation for the building stock in Isfahan. Part I: exposure and vulnerability.” *Bulletin of Earthquake Engineering*, 19(4), 1709-1737. <https://doi.org/10.1007/s10518-020-01036-2>
- Kohrangi, M., Bazzurro, P., & Vamvatsikos, D. 2021. “Seismic risk and loss estimation for the building stock in Isfahan: part II: hazard analysis and risk assessment.” *Bulletin of Earthquake Engineering*, 19(4), 1739-1763. <https://doi.org/10.1007/s10518-020-01037-1>
- Kohrangi, M., P. Bazzurro, D. Vamvatsikos, and A. Spillatura. 2017. “Conditional spectrum-based ground motion record selection using average spectral acceleration.” *Earthquake Engineering & Structural Dynamics*, 46 (10): 1667–1685. <https://doi.org/10.1002/eqe.2876>
- Kohrangi, M., Bazzurro, P., & Vamvatsikos, D. 2016. “Vector and scalar IMs in structural response estimation, Part I: Hazard analysis.” *Earthquake Spectra*, 32(3), 1507-1524. <https://doi.org/10.1193/053115EQS080M>
- Kohrangi, M., Bazzurro, P., & Vamvatsikos, D. 2016. “Vector and scalar IMs in structural response estimation, part II: building demand assessment.” *Earthquake Spectra*, 32(3), 1525-1543. <https://doi.org/10.1193/053115EQS081M>
- Krausmann, E., and A. M. Cruz. 2021. “Natech risk management in Japan after Fukushima – What have we learned?” *Loss Prevention Bulletin*, 277. <https://www.icheme.org/media/15301/krausmannnew.pdf>
- Kwon, O. S., and A. Elnashai. 2006. “The effect of material and ground motion uncertainty on the seismic vulnerability curves of RC structure.” *Engineering Structures*, 28 (2): 289–303. <https://doi.org/10.1016/j.engstruct.2005.07.010>
- Liu, J. B. 2017. “Finite element analysis of the integral hoisting of 49m flange connection flare.” In *Proc., IOP Conference Series: Materials Science and*

- Engineering*, 281 (1): 012049. Busan, Korea. <https://doi.org/10.1088/1757-899X/281/1/012049>
- López, A., V. Cepeda, and J. Mendoza. 1996. "Dynamic analysis of slender steel distillation towers." In *Proc., Eleventh World Conference on Earthquake Engineering*. Acapulco, Mexico.
- Mander, J. B., M. J. Priestley, and R. Park. 1988. "Theoretical stress-strain model for confined concrete." *Journal of Structural Engineering*, 114 (8): 1804–1826. [https://doi.org/10.1061/\(ASCE\)0733-9445\(1988\)114:8\(1804\)](https://doi.org/10.1061/(ASCE)0733-9445(1988)114:8(1804))
- McKenna, F., and G. L. Fenves. 2011. *The OpenSees Command Language Manual (1.2 edn)*. Berkeley, CA: University of California Berkeley.
- Moharrami, H., and M. A. Amini. 2014. "Seismic vulnerability assessment of process towers using fragility curves." *The Structural Design of Tall and Special Buildings*, 23 (8): 593–603. <https://doi.org/10.1002/tal.1067>
- Papadaki, C. I., Chatzopoulou, G., Sarvanis, G. C., & Karamanos, S. A. 2018. "Buckling of internally-pressurized spiral-welded steel pipes under bending." *International Journal of Pressure Vessels and Piping*, 165, 270-285. <https://doi.org/10.1016/j.ijpvp.2018.07.006>
- Patkas, L. A., and S. A. Karamanos. 2007. "Variational solutions for externally induced sloshing in horizontal-cylindrical and spherical vessels." *Journal of Engineering Mechanics (ASCE)*, 133 (6): 641–655. [https://doi.org/10.1061/\(ASCE\)0733-9399\(2007\)133:6\(641\)](https://doi.org/10.1061/(ASCE)0733-9399(2007)133:6(641))
- Phan, H. N., F. Paolacci, R. Di Filippo, and O. S. Bursi. 2020. "Seismic vulnerability of above-ground storage tanks with unanchored support conditions for Na-tech risks based on Gaussian process regression." *Bulletin of Earthquake Engineering*, 18: 6883–6906. <https://doi.org/10.1007/s10518-020-00960-7>
- Qiu, Y., C. Zhou, and A. Siha. 2020. "Correlation between earthquake intensity parameters and damage indices of high-rise RC chimneys." *Soil Dynamics and Earthquake Engineering*, 137: 106282. <https://doi.org/10.1016/j.soildyn.2020.106282>
- Sheng, X., H. Zhang, Y. Bao, and C. Ling. 2016. "Finite element checking of flange connection in integral hoisting of flare stack." In: *Proc., 2016 International Conference on Advanced Electronic Science and Technology (AEST 2016)*, 380–386. Shenzhen, China: Atlantis Press. <https://doi.org/10.2991/aest-16.2016.50>
- Silva, V., S. Akkar, J. W. Baker, P. Bazzurro, J. M. Castro, H. Crowley, M. Dolsek, C. Galasso, S. Lagomarsino, R. Monteiro, D. Perrone, K. Pitilakis, D. Vamvatsikos D. 2019. "Current challenges and future trends in analytical fragility and vulnerability modelling." *Earthquake Spectra*, 35 (4): 1927–1952. <https://doi.org/10.1193/042418EQS1010>
- Silva, V., H. Crowley, H. Varum, R. Pinho, and R. Sousa. 2014. "Evaluation of analytical methodologies used to derive vulnerability functions." *Earthquake Engineering & Structural Dynamics*, 43 (2): 181–204. <https://doi.org/10.1002/eqe.2337>
- Sousa, R., Almeida, J. P., Correia, A. A., and Pinho, R. (2020). "Shake table blind prediction tests: Contributions for improved fiber-based frame modelling." *Journal of Earthquake Engineering*, 24(9), 1435–1476. <https://doi.org/10.1080/13632469.2018.1466743>

- Spritzer, J. M., and S. Guzey. 2017. "Review of API 650 Annex E: Design of large steel welded aboveground storage tanks excited by seismic loads." *Thin-Walled Structures*, 112: 41–65. <https://doi.org/10.1016/j.tws.2016.11.013>
- Taillon, J. Y., Légeron, F., & Prud'homme, S. (2012). "Variation of damping and stiffness of lattice towers with load level." *Journal of Constructional Steel Research*, 71, 111–118. <https://doi.org/10.1016/j.jcsr.2011.10.018>
- Tsantaki, S., and C. Adam. 2013. "Collapse capacity spectra based on an improved intensity measure." In: *Proc., 4th ECCOMAS Thematic Conference on Computational Methods in Structural Dynamics and Earthquake Engineering (COMPDYN 2013)*. Kos, Greece. <https://doi.org/10.7712/120113.4510.C1382>
- United Nations. 2015. *Sendai Framework for Disaster Risk Reduction 2015 - 2030*. Geneva, Switzerland. www.unisdr.org
- Vamvatsikos, D., & Cornell, C. A. 2005. "Developing efficient scalar and vector intensity measures for IDA capacity estimation by incorporating elastic spectral shape information." *Earthquake Engineering & Structural Dynamics*, 34(13), 1573–1600. <https://doi.org/10.1002/eqe.496>
- Vamvatsikos, D., and C. A. Cornell. 2004. "Applied incremental dynamic analysis." *Earthquake Spectra*, 20 (2): 523–553. <https://doi.org/10.1193/1.1737737>
- Vamvatsikos, D., and C. A. Cornell. 2002. "Incremental dynamic analysis." *Earthquake Engineering & Structural Dynamics*, 31 (3): 491–514. <https://doi.org/10.1002/eqe.141>
- Vathi, M., S. A. Karamanos, I. A. Kapogiannis, and K. V. Spiliopoulos. 2017. "Performance Criteria for Liquid Storage Tanks and Piping Systems Subjected to Seismic Loading." *Journal of Pressure Vessel Technology (ASME)*, 139 (5): 051801. <https://doi.org/10.1115/1.4036916>
- Wang, L., and X. Y. Fan. 2019. "Failure cases of high chimneys: A review." *Engineering Failure Analysis*, 105: 1107–1117. <https://doi.org/10.1016/j.engfailanal.2019.07.032>
- Wilson, J. L. 2003. "Earthquake response of tall reinforced concrete chimneys." *Engineering Structures*, 25 (1): 11–24. [https://doi.org/10.1016/S0141-0296\(02\)00098-6](https://doi.org/10.1016/S0141-0296(02)00098-6)
- Yu, C.-C., and A. S. Whittaker. 2021. "Review of analytical studies on seismic fluid-structure interaction of base-supported cylindrical tanks." *Engineering Structures*, 233: 111589. <https://doi.org/10.1016/j.engstruct.2020.111589>
- Zhang, Z., J. Park, O.-S. Kwon, A. Sextos, E. Strepelias, N. Stathas, and S. Bousias. 2021. "Hybrid simulation of structure-pipe-structure interaction within a gas processing plant." *Journal of Pipeline Systems Engineering and Practice (ASCE)*, 12 (2): 04020073. [https://doi.org/10.1061/\(ASCE\)PS.1949-1204.0000526](https://doi.org/10.1061/(ASCE)PS.1949-1204.0000526)
- Zhou, C., M. Tian, and K. Guo. 2019. "Seismic partitioned fragility analysis for high-rise RC chimney considering multidimensional ground motion." *The Structural Design of Tall and Special Buildings*, 28 (1): e1568. <https://doi.org/10.1002/tal.1568>
- Zhou, C., X. Zeng, Q. Pan, and B. Liu. 2015. "Seismic fragility assessment of a tall reinforced concrete chimney." *The Structural Design of Tall and Special Buildings*, 24 (6): 440–460. <https://doi.org/10.1002/tal.1173>

STATEMENTS AND DECLARATIONS

Funding

The financial support from the European Union's Horizon 2020 research and innovation programmes "INFRASTRESS-Improving resilience of sensitive industrial plants & infrastructures exposed to cyber-physical threats, by means of an open testbed stress-testing system" under Grant Agreement No. 833088, "HYPERION – Development of a Decision Support System for Improved Resilience & Sustainable Reconstruction of historic areas to cope with Climate Change & Extreme Events based on Novel Sensors and Modelling tools" under Grant Agreement No. 821054 and "HARMONIA – Development of a Support System for Improved Resilience and Sustainable Urban areas to cope with Climate Change and Extreme Events based on GEOSS and Advanced Modelling Tools" under Grant Agreement No. 101003517 is gratefully acknowledged.

Competing Interests

The authors have no relevant financial or non-financial interests to disclose.

Data Availability

Some or all data, models, or code that support the findings of this study are available from the corresponding author upon reasonable request.